CO2 Utilization in Built Environment via the PCO2 Swing Carbonation of Alkaline Solid Wastes with Different Mineralogy

Journal:	*Faraday Discussions*
Manuscript ID	FD-ART-03-2021-000022
Article Type:	Paper
Date Submitted by the Author:	01-Mar-2021
Complete List of Authors:	Rim, Guanhe; Columbia University, Earth and Environmental Engineering; Columbia University, Lenfest Center for Sustainable Energy, The Earth Institute Roy, Noyonika; Columbia University, Department of Chemical Engineering; Columbia University, Lenfest Center for Sustainable Energy Zhao, Diandian; Columbia University, Department of Civil Engineering and Engineering Mechanics; Columbia University, Lenfest Center for Sustainable Energy Kawashima, Shiho; Columbia University, Stallworth, Phillip; Hunter College, Greenbaum, Steve G.; Hunter College, Chemistry and Biochemistry Park, Ah-Hyung; Columbia University, Department of Earth and Environmental Engineering & Department of Chemical Engineering

SCHOLARONE™
Manuscripts

CO$_2$ Utilization in Built Environment via the Pco$_2$ Swing Carbonation of Alkaline Solid Wastes with Different Mineralogy

Guanhe Rim[a,b,c], Noyonika Roy[b,c], Diandian Zhao[b,d], Shiho Kawashima[b,d], Phillip Stallworth,[e]

Steven G. Greenbaum,[e] and Ah-Hyung Alissa Park[a,b,c,*]

[a]Department of Earth and Environmental Engineering,

[b]Lenfest Center for Sustainable Energy, The Earth Institute, Columbia University, NY 10027, United States

[c]Department of Chemical Engineering, Columbia University, NY 10027, United States

[d]Department of Civil Engineering and Engineering Mechanics, Columbia University, New York 10027, USA

[e]Department of Physics & Astronomy, Hunter College of the City University of New York, New York, NY, 10065, USA

* Corresponding author - E-mail address: ap2622@columbia.edu

ABSTRACT

Carbon mineralization to solid carbonates is one of the reaction pathways that can not only utilize captured CO_2 but also potentially store them in the long term. In this study, the dissolution and carbonation behaviors of alkaline solid wastes (i.e., waste concrete) was investigated. Concrete is one of the main contributors to a large carbon emission in built environment. Thus, the upcycling of waste concrete via CO_2 utilization has multifaceted environmental benefits including CO_2 emission reduction, waste management and reduced mining. Unlike natural silicate minerals such as olivine and serpentine, alkaline solid wastes including waste concrete are highly reactive, and thus, their dissolution and carbonation behaviors vary significantly. Here, both conventional acid (e.g., hydrochloric acid) and less studied carbonic acid (i.e., CO_2 saturated water) solvent systems were explored to extract Ca from concrete. Non-stoichiometric dissolution behaviors between Ca and Si were confirmed under far-from-equilibrium condition (0.1 wt.% slurry density) and the re-precipitation of the extracted Si was observed at near-equilibrium condition (5 wt.% slurry density), when the Ca extraction was performed at a controlled pH of 3. These experiments with a wide range of slurry densities provided valuable insights into Si re-precipitation phenomena and its effect on the mass transfer limitation during concrete dissolution. Next, the use of the partial pressure of CO_2 for the pH swing carbon mineralization process was investigated for concrete and the results were compared to those of Mg-bearing silicate minerals. In the P_{CO_2} swing process, the extraction of Ca was significantly limited by the precipitation of the carbonate phase (i.e., calcite), since CO_2 bubbling could not provide a low enough pH condition for concrete-water-CO_2 systems. Thus, this study showed that the two-step carbon mineralization via P_{CO_2} swing, that has been developed for Mg-bearing silicate minerals, may not be viable for highly reactive Ca-bearing silicate materials (e.g., concrete). The precipitated calcium carbonate (PCC) derived from waste

concrete via a pH swing process showed very promising results with a high CO_2 utilization potential as an upcycled construction material.

KEYWORDS

CO_2 utilization, Carbon mineralization, Built environment, Waste concrete, P_{CO_2} swing, Mineral dissolution

Introduction

Climate change has become a significant global environmental issue in recent decades. Human activities have been contributing to a great amount of carbon dioxide (CO_2) and other greenhouse gases (GHG) emissions. According to the International Panel on Climate Change (IPCC), the atmospheric CO_2 concentration may increase to 570 ppm, with an average rise in 1.9 ℃ global temperature by 2100, resulting in natural disasters such as extreme weather change and sea-level rise.[1] Thus, the goal of controlling the global temperature increase to 2 ℃ above pre-industrial levels by 2100 is generally accepted as the appropriate target. In order to achieve this goal, it is predicted that a 50 − 85% reduction of GHG emissions from the current level is required.[1] Thus, enormous global efforts have been placed on the development of Carbon Capture, Utilization, and Storage (CCUS) to mitigate CO_2 emissions in the immediate future.

Ex-situ carbon mineralization, which mimics natural weathering processes between silicate minerals and CO_2, is one of the most eminent CCUS technologies. The proposed process combines CO_2 capture with the production of value-added materials, which are thermodynamically stable

solid carbonates.[2-4] In the *Ex-situ* carbon mineralization, magnesium silicate minerals, such as serpentine ($Mg_3Si_2O_5(OH)_4$), are generally used because of their abundance in the world (see **Fig. 1**). Large amounts of silicate minerals exist, which can sequester all fossil fuel-bound carbon in the future[5] but the carbon mineralization pathway of CCUS is currently challenged due to high parasitic energy consumption for mining processing and the need for mining. In terms of reaction rates and extents, the overall carbon mineralization process is thermodynamically favored but often limited by the mineral dissolution step due to the low reactivity of natural silicate minerals. Thus, a number of pre-treatment options (both physical and chemical) have been considered to activate natural Mg-bearing silicate minerals.[6-13]

As shown in **Fig. 1**, in addition to natural silicate minerals, alkaline industrial solid wastes including fly ash, waste concrete, and steel slag, can be used to fix gaseous CO_2 into solid carbonates because of their high Ca and Mg content.[14-25] Due to the high reactivity of industrial silicate waste materials, rapid carbon mineralization will be viable without the energy-intensive pretreatment of feedstock materials. It is also expected that the use of these industrial wastes, which often coexist with industrial CO_2 point sources (e.g., iron and steel slag at steel manufacturing plants emitting a large amount of CO_2), can eliminate the energy-intensive transportation of solid feedstocks for carbon mineralization. In the past, the carbonation of fly ash and steel slag have been extensively studied; however, less attention was given to waste concrete. Recently, the potential utilization of waste concrete for carbon mineralization has been explored.[26] The waste concrete mainly consists of $Ca(OH)_2$ and calcium silicate hydrates (C–S–H). In the presence of CO_2 and water, carbonic acid is produced and reacted with alkali from the cement to form $CaCO_3$. Thus, *Ex-situ* carbon mineralization with the waste concrete would offer an opportunity to produce

value-added carbonation products that can be used to close the calcium and carbon cycles within
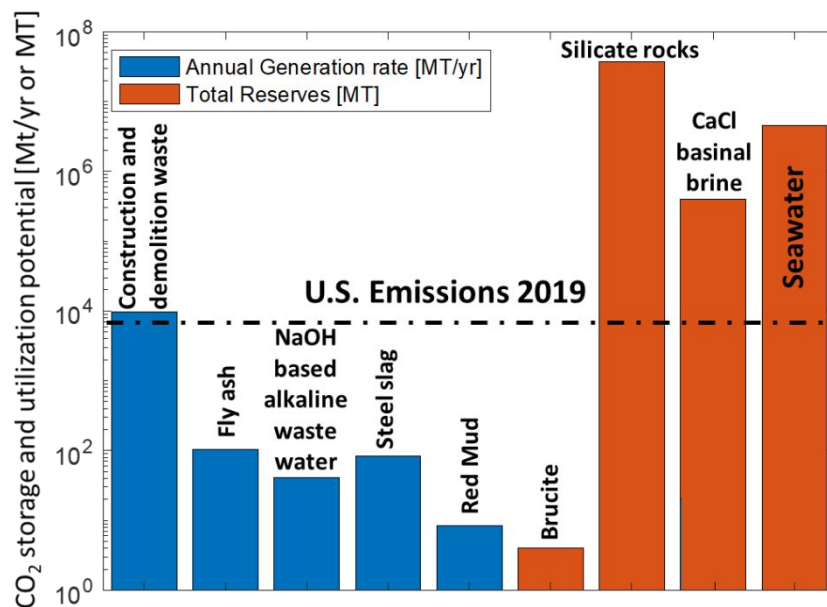
the built environment.

Fig. 1 CO_2 storage and utilization potential of various feedstocks via carbon mineralization.[20,27-30]

Carbon mineralization can be performed in a single step or two-step process. While a single

step carbon mineralization requires a lower energy consumption, it does not allow the formation

of high-quality products. Thus, a two-step pH swing process has been developed for step-wise

extraction of Ca and Mg to produce high purity carbonates with controlled morphological

structures and chemistries.[31] The conventional design of pH swing processes[32, 33] use acids and

bases to achieve both rapid metal (Ca and Mg) extraction from silicate materials favored at low

pH and subsequent metal-carbonation reaction favored a high pH. Unfortunately, the need for acids

and bases has limited the technical and economic feasibility of pH swing carbon mineralization

technologies. Thus, carbon mineralization via P_{CO_2} swing has been theorized to reduce the

consumption of acid and base.[13, 34, 35]

The two-step P_{CO_2} swing carbon mineralization, which uses a CO_2-containing gas stream as a proton (H^+) source, could be quite complex as illustrated in **Fig. 2(a)**. This process consists of various dissolution and precipitation steps of different elements. First, Ca and/or Mg are extracted from silicate materials in a gas-liquid-solid three-phase system. The CO_2-containing gas stream ($P_{CO_2} \leq 1$ atm) is bubbled into the slurry to generate carbonic acid (H_2CO_3) via CO_2 hydration. Then, Ca and/or Mg are leached from the silicate materials by rapid ion exchange between metal ions (Mg^{2+} or Ca^{2+}) and H^+ (from H_2CO_3) in the aqueous phase. After the mineral dissolution step, the pH of the Ca/Mg-rich (also CO_2 saturated) solution is subsequently increased by degassing CO_2. The pH of the precipitation reactor should be at a level where CO_3^{2-} ions prevail to induce the precipitation of extracted Ca^{2+} and Mg^{2+}. The pH swing via CO_2 degassing can be achieved by bubbling a relatively low P_{CO_2} gas stream such as air (410 ppm CO_2) into the precipitation reactor. The advantages of the two-step P_{CO_2} swing process include that acid and base are not required, the operating conditions of the two steps can be independently optimized, and high-purity final products can be obtained.[36]

Another option to improve the overall sustainability of the carbon mineralization technology is the integration of renewable energy. With a rapid decrease in the price of renewable electricity and its increased availability, there is now a unique opportunity to use renewable energy to convert and store carbon. For instance, renewable electric energy can be used to generate concentrated acids and bases which could lower costs making *Ex-situ* carbon mineralization more economically viable. Electromembrane technologies, including electrodialysis with bipolar membranes (EDBM), have been studied to produce concentrated acid (HCl) and base (NaOH) utilizing renewable electric energy and brines.[37-41] The most recent EDBM study reported that 3.3 mol/L of HCl and 3.6 mol/L of NaOH are obtained with variable current intensity (mimic the use of PV

solar energy) and brines (highly concentrated NaCl solution).[37] These strong acids and bases can

be used in *ex-situ* carbon mineralization as illustrated in **Fig. 2(b)**, and the overall technology will

become sustainable, while allowing rapid mineral dissolution and carbonation via the pH swing

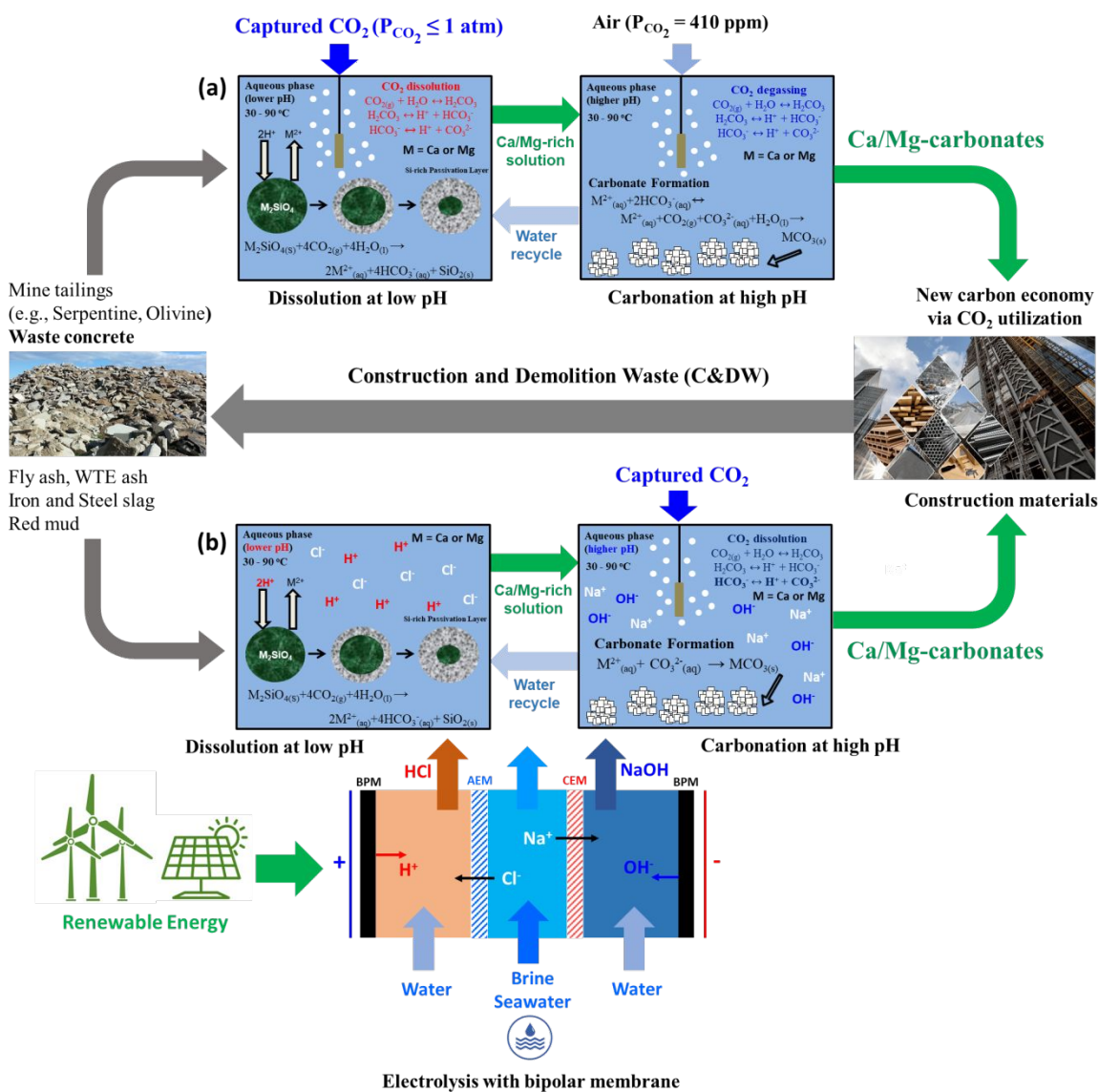process, and will produce high value-materials.

Fig. 2 Carbon mineralization of alkaline industrial wastes and silicate minerals **(a)** via P_{CO_2} swing

and **(b)** via pH swing using acid and base generated from electrolysis with a bipolar membrane

system.

This study aimed to investigate the carbon mineralization behaviors of waste concrete via these two options: P_{CO_2} swing and strong acid/based produced using renewable energy. The results were then compared to previously studied carbonation of serpentine, a Mg-bearing silicate mineral. The Ca, Mg, and Si extraction behaviors were investigated as a function of temperature and slurry density. After the leaching step, solid carbonate was precipitated via pH shift through two methods: CO_2 degassing and the addition of base (NaOH). Finally, the value-added product of the CO_2 mineralization process, precipitated calcium carbonate (PCC), was tested as a replacement for Ordinary Portland Cement (OPC) to evaluate its CO_2 utilziation potential. The findings from this study provided imporatnt kinetic and mechanistic insights into how CO_2 can be fixed into the solid carbonate phase using Ca and Mg-bearing silicate materials, including waste concrete, via the pH swing carbon mineralization process. The findings show implications for how CO_2 utilization can play a key role in the improved sustainability of the built environmnet.

Materials and methods

Hydrated cement

In order to perform controlled experiments, concrete samples were prepared by hydrating Ordinary Portland Cement (OPC), which underwent curing for 7 days. The hydrated cement represents the reactive materials of freshly demolished waste concrete, excluding the weathered surface concrete. The hydrated cement was then ground and sieved to the size range of 125 to 210 μm. According to literature references, hydrated cement consists of three major components – Calcium Silicate Hydrate (C-S-H) gel, calcium hydroxide ($Ca(OH)_2$), and Ettringite ($Ca_6Al_2(SO_4)_3(OH)_{12} \cdot 26H_2O$) with minor percentages of unreacted clinker (calcium silicate), calcium carbonates (due to aging), and a complex form of alumina.[42] The average amount of

calcium oxide is reported to be about 60% of the total weight.[42] The surface area of hydrated cement samples was determined using BET analysis (BET analyzer – Nova e-Series, Quantachrome, Boynton Beach, FL) and was found to be 49.12 m²/g. ICP analysis was performed on the hydrated cement sample fully digested in 5% HNO_3 after fusing it with lithium metaborate to determine its elemental composition and the results are shown in **Table 1**. The Ca and Si contents in prepared hydrated cement samples were 44.0 wt.% and 14.0 wt.%, respectively.

Table 1. Elemental compositions of the hydrated cement and activated serpentine.

Feedstock	Ca [wt.%]	Mg [wt.%]	Al [wt.%]	Fe [wt.%]	Si [wt.%]	Analysis Method
Hydrated cement	44.0	0.0	1.3	2.3	14.0	ICP
Activated serpentine	0.5	23.0	1.5	7.0	20.5	XRF

Activated serpentine mine tailing

Serpentine is hydrous magnesium silicate mineral that has been extensively studied for carbon mineralization, since a massive amount of serpentine mine tailing exists with a high CO_2 storage potential. Raw serpentine is not very reactive, since it is mostly in a stable silicate form. Thus, serpentine was activated via heat treatment to create different silicate structures and its dissolution and carbonation behaviors were compared to those of hydrated cement in order to investigate the effect of mineralogy on the carbon mineralization behaviors. Activated serpentine used in this study was in the form of < 100 μm particles. The particle size distribution of the sample was determined through the laser diffraction measurement (LSTM 13320 MW, Beckman Coulter Inc. Brea, CA). The BET surface area was 31.95 m²/g (BET analyzer – Nova e-Series, Quantachrome, Boynton Beach, FL). The chemical composition of the activated serpentine was determined via a Wavelength Dispersion X-ray Fluorescence (WD-SRF, Panalytical Axios) and its major

components were found to be MgO, FeO, and SiO_2. As shown in **Table 1**, the amounts of Mg and Si in the activated serpentine samples were 23.2 wt.% and 20.5 wt.%, respectively.

Extraction of Ca and Mg from alkaline solid wastes

The dissolution studies of the alkaline solid wastes, hydrated cement and activated serpentine, were conducted in a semi-batch reactor. The reactor was a 500 ml 3-neck flask, which was equipped with a thermocouple, a pH probe, a condenser, and a gas sparger. In the case of the P_{CO_2} swing process, 300 ml of deionized (D.I.) water was charged into the semi-batch reactor and pure CO_2 (P_{CO_2} = 1 atm) was bubbled into the D.I. water at a constant flow rate of 150 ml/min to form the solvent that was fully saturated with CO_2 to provide carbonic acid as the proton source. After the water-CO_2 system reached equilibrium (denoted by a stabilized pH around 3.9), the alkaline solid waste sample was charged to the reactor and the time was marked as the start of the dissolution experiment. The given CO_2 flow rate was maintained during the entire reaction period. In the case of acid leaching, pH 3 HCl solution was used. To maintain the solution pH during the leaching experiment, concentrated HCl solution was continuously added to the reactor system. The total amount of added concentrated HCl solution was varied from 2 ml to 10 ml depending on the slurry density (solid to liquid ratio).

The stirring rate of the leaching system was set at 900 rpm for all experiments to ensure that the reactions can be performed without the bluk mass transfer issues. The pH profile of the solution was recorded every 3 seconds and the reaction temperature was controlled by an electrical heater and was maintained at a target temperature throughout each experiment. During the leaching experiment, approximately 300 μL of slurry samples were taken at a set sample interval. The slurry samples were then quickly filtered by 0.2 μm filters and the filtrate was diluted using 2% HNO_3 to stop any potential reactions. After dilution, liquid samples were analyzed for the elemental

concentrations (i.e., Ca, Mg, and Si) using the Inductively Coupled Plasma Optical Emission Spectroscopy (ICP-OES) and the results were used to determine the dissolution kinetics of the silicate solid waste materials.

The first set of experiments were performed using two slurry density conditions (0.1 and 1 wt.%) at 22, 30, 60, and 90 °C to investigate the effect of temperature on the elemental extraction behaviors of hydrated cement and activated serpentine mine tailing. Higher slurry densities (3 wt.%, 5 wt.%, and 10 wt.%) were subsequently studied to study the dissolution behaviors of these alkaline solid wastes at near-equilibrium conditions. At the end of each dissolution experiment, the slurry was filtered to separate solid residue particles. The solids were washed multiple times with D.I. water and ethanol, and dried in a vacuum oven at 70 °C overnight. The dried solid samples were analyzed by a Carbon Analyzer (CA) to determine the presence of carbonate phases.

Precipitation of solid carbonates

The extracted Ca and Mg were next carbonated and solid carbonates were formed. In case of the P_{CO_2} swing process, the precipitation of solid metal-carbonates was carried out by degassing CO_2 out of the filtrate (liquid phase) from the dissolution step. The same reactor setup was used and the reaction temperature was varied from 30 to 60 °C under ambient pressure. Air ($P_{CO_2} = 400$ ppm) was bubbled into the CO_2 saturated Ca or Mg-rich solution at a constant flow rate of 500 mL/min and the solution pH was continuously monitored. As the dissolved CO_2 was degassed by bubbling air, the pH of the solution increased up to 8.5 - 9.5. The pH and temperature swing induced the precipitation of Ca and Mg-carbonates. In case of the acid (pH 3 HCl) leaching process, pure CO_2 ($P_{CO_2} = 1$ atm) was bubbled into the leachate at a rate of 30 ml/min, while maintaining the solution pH at 9 by continuously adding 50 wt.% NaOH solution.

At the end of the precipitation step, the slurry was filtered to collect the Ca and Mg-carbonate particles, and they were washed with D.I. water and ethanol several times. The washed carbonate particles were dried in a vacuum oven at 70 °C overnight for further analysis. In order to identify the precipitated carbonate phases, the X-ray diffraction patterns of the solid particles were collected in the range of 5-70° 2θ with a step size of 0.05° and a scan time of 0.5 s using the X-ray Powder Diffraction (X2, Scintag, Inc.). The solid particles were also analyzed by TGA (LABSYS Evo TGA) in order to quantify different carbonate phases. TGA thermal decomposition curves of each sample were obtained in N_2 with a heating rate of 10 °C.

Hydration behaviors of cement containing precipitated calcium carbonate

In order to reduce the carbon intensity of building materials, it is important to find alternative materials for cements and concrete. As discussed earlier, precipitated calcium carbonate (PCC) produced from the carbonation of alkaline solid wastes is one of the potential candidates to significantly reduce the carbon footprints of concrete. It is, however, very important to ensure that the performance of produced concrete can be maintained as the PCC is incorporated into the mix. One of the tests that can be performed to evaluate the quality of the produced cement is the measurements of the heat of hydration. In this study, the hydration behaviors of cement mixes containing 10 wt.% (CC10), 20 wt.% (CC20), and 30 wt.% (CC30) of PCC as a replacement for Ordinary Portland cement (OPC) were investigated. The PCC produced from our study was mixed with other cement materials and distilled water, and these cement pastes were set at a water-to-binder ratio of 0.4 by weight. All ingredients were weighed and mixed together using a mixer, where the total weight of the solid materials for each cement batch was 10 g. During cement curing reaction, the heat of hydration of cement pastes was measured in an isothermal calorimeter by monitoring the heat flow generated at a constant temperature of 25 °C. For each sample,

approximately 5 g of fresh cement paste containing our PCC was added to a glass ampoule and placed in the calorimeter. The heat flow was measured over a period of 48 – 96 hours, depending on how long it took to reach stabilization.

Results and Discussion

Dissolution behaviors of hydrated cement at pH 3

The effect of temperature on Ca and Si extraction behaviors of the hydrated cement was studied at far-from-equilibrium condition (0.1 wt.% slurry density) at pH 3. The reaction temperatures were varied from 22, 60, to 90 °C. **Fig. 3 (a)** shows the elemental concentration profiles of dissolved species. From the Ca concentration profiles it is observed that the initial Ca extraction kinetics and their contributions to the overall extents of Ca extraction increased with temperature. However, the Si concentration profiles in the bulk solution were almost identical for all temperature conditions indicating that the effect of temperature on Si extraction was insignificant.

The Ca/Si concentration ratios during the far-from-equilibrium dissolution experiments at 22, 60, and 90 °C were plotted in **Fig. 3(c)**. The Ca/Si concentration ratios (C_{Ca}/C_{Si}) were higher than their compositional ratio in the starting material, hydrated cement, indicating the incongruent dissolution behavior, which is strong evidence of the formation of a Si-rich ash layer on the surface of the dissolving particles.[43] These types of incongruent, non-stoichiometric (between Ca and Si or Mg and Si), dissolution behaviors have been reported for silicate minerals such as serpentine under acidic condition (e.g., HNO_3 solvent) and explained by the weaker Metal-O bonds compared to the Si-O bonds.[44-46] The rapid ion exchange reaction ($M^{2+} \leftrightarrow 2H^+$) leads to the formation of a silanol group rich layer on the reacting surface.[44-46] These silanol groups are condensed to form

oxide bonds and a Si-rich passivation layer is formed.[45, 46] The extraction of alkaline metal (Ca or Mg) is often limited by the formation of this Si-rich passivation layer on the reactive surface during the dissolution of Ca and Mg-bearing silicate minerals.[44, 47-50]
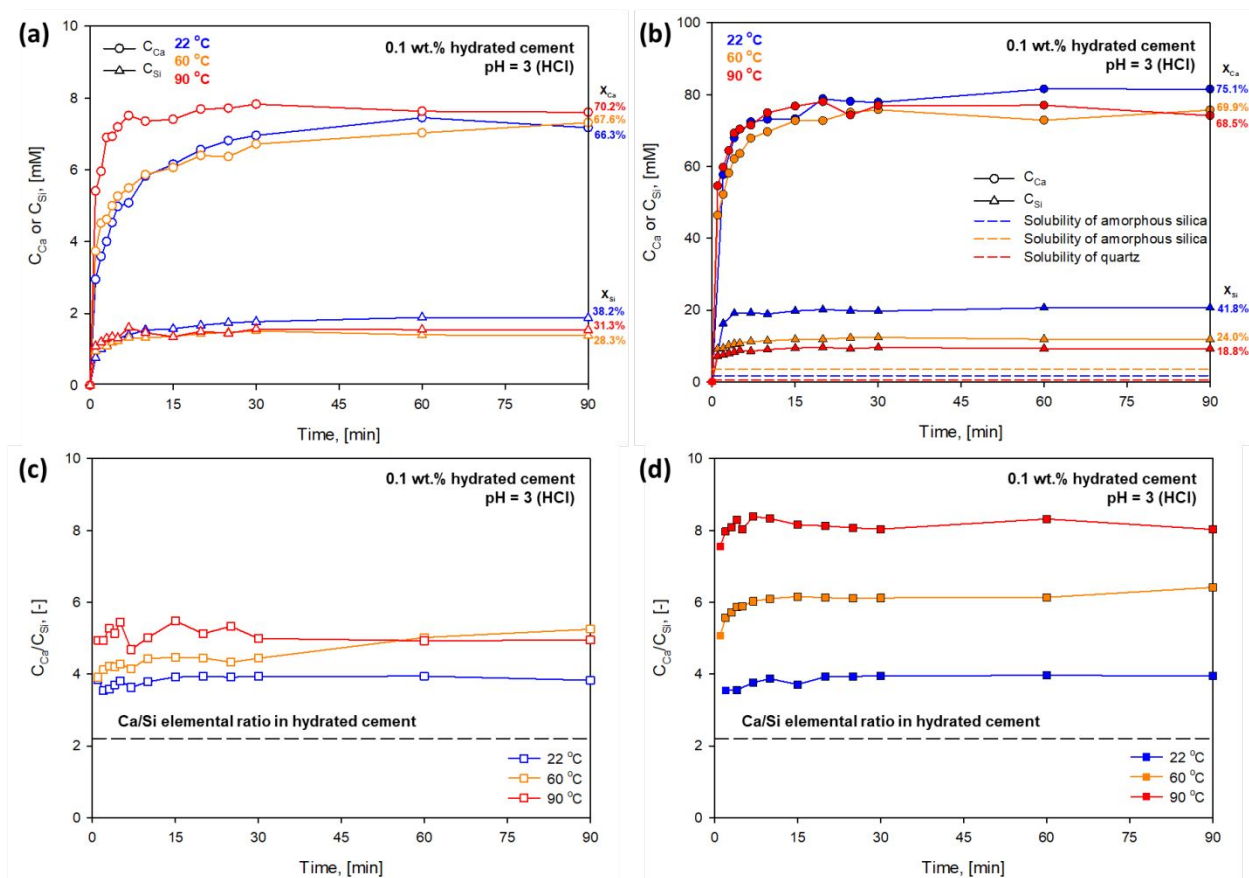

Fig. 3. Effect of reaction temperature on the dissolution of hydrated cement: (a) Ca and Si concentrations and (c) C_{Ca}/C_{Si} profile for 0.1 wt.% slurry density case, and (b) Ca and Si concentrations and (d) C_{Ca}/C_{Si} profile for 1 wt.% slurry density case.

Interestingly, it was observed that the degree of the incongruent dissolution of hydrated cement was affected by reaction temperature. As shown in **Fig. 3(c)**, at 90 °C, the dissolution behavior was slightly more incongruent compared to 60 °C and 22 °C cases. Regardless, the overall yields of the Ca extraction from hydrated cement were very high (between 66.3% and 70.2%).

These results suggest that the Si-rich layer was formed on the surface of hydrated cement particles, but the mass transfer limitation through that Si-rich ash layer was not significant enough to reduce the overall Ca and Si dissolution rates. This phenomenon is quite different from that of natural Ca and Mg-bearing silicate minerals, where the Si-rich surface layer significantly reduces the extent of Ca and Mg extraction and controls the overall mineral dissolution kinetics.[32, 51] These differences suggest the presence of distinct pore sizes and pore networks with in the Si-rich ash layer of dissolved hydrated concrete and silicate minerals. Even with a thicker ash layer, the hydrated cement particles continued to dissolve. The time required to reach 70.2% Ca extraction at 90 °C was about 5 minutes, which suggests that the Ca recovery from waste concrete is very promising for its upcycling via CO_2 utilization.

The effect of reaction temperature on the dissolution of hydrated cement was further investigated at a higher slurry density of 1 wt.%, and the results are shown in **Fig. 3(b)** and **3(d)**. As shown in **Fig. 3(b)**, the 1 wt.% slurry density condition shows different Si extraction behaviors from the far-from-equilibrium conditions (**Fig. 3(a)**). It was confirmed that the extents of Si extraction decreased with increasing temperature up to 90 ℃. The decreased extents of Si extraction were likely attributed to the re-precipitation of extracted Si because the silica phase is insoluble under acidic conditions. An empirical observation has been reported that amorphous silica, which is a relatively soluble Si phase, precipitated at lower temperatures (≤ 60 °C) and the precipitation of quartz, which is a less soluble and thermodynamically stable Si phase, was favored at higher temperatures.[13] The solubility limits of amorphous silica and quartz at each reaction temperature are given as comparisons in **Fig. 3(b)**, and they show that Si was supersaturated at all temperature conditions with respect to amorphous silica or quartz indicating the strong possibility of Si re-precipitation. At lower reaction temperatures (22 °C), a higher Si concentration profile

was obtained with respect to the other temperature conditions. This suggests that the re-precipitation rates of both amorphous silica (kinetically favored Si phase) and quartz were slow. Thus, the effect of Si-reprecipitation on the passivation effect was more significant with increasing temperature.[52]

The enhanced Si-reprecipitation behaviors at increased reaction temperatures resulted in a net reduction in the Ca extraction at 1 wt.% of slurry density (near equilibrium) condition. In contrast with the far-from-equilibrium condition (0.1 wt.% slurry density, **Fig. 3(a)**), the extents of Ca extraction as well as the initial Ca leaching rates at 22, 60, and 90 ℃ were almost identical as shown in **Fig. 3(b)**. Again, the reduced temperature effect on the Ca extraction from hydrated cement could be explained by the faster re-precipitation of Si phases (amorphous silica and/or quartz) on the reactive surface at higher temperatures and increased slurry densities.[34, 52, 53] Daval et al.[47] reported that the strongly inhibited dissolution of olivine at 90 ℃ was caused by the formation of an amorphous silica layer on the mineral surface. Others also showed that the passivation effect of the precipitated amorphous silica was enhanced with increasing temperature due to its densification at higher temperature conditions.[34, 54] The Ca/Si concentration ratios shown in **Fig. 3(d)** clearly suggest the enhanced incongruent dissolution behaviors of hydrated cement at elevated temperature conditions. The C_{Ca}/C_{Si} of 1 wt.% slurry density cases dramatically increased with temperature from $C_{Ca}/C_{Si} = 3.8$ at 22 ℃ to $C_{Ca}/C_{Si} = 8.0$ at 90 ℃ showing significantly intensified incongruent dissolution behaviors of hydrated cement.

In order to obtain a highly concentrated Ca-rich solution for the subsequent carbonation step, the slurry density was further increased up to 5 wt.%. Since hydrated cement was found to be very reactive even at room temperature (22 ℃), subsequent dissolution experiments were performed at 22 ℃ in order to minimize the energy requirement for the Ca extraction from hydrated

cement. The C_{Ca}, C_{Si}, and C_{Ca}/C_{Si} profiles were acquired for the hydrated cement dissolution at higher slurry densities. As shown in **Fig. 4(a)**, a highly concentrated Ca-rich solution was obtained by increasing the slurry density from 1 to 5 wt.%. The highest achieved C_{Ca} was 332.0 mM at 5 wt.% slurry density condition, but there was a tradeoff of in regards to reduced extent of Ca extraction (X_{Ca}) at higher slurry densities. Si continued to be supersaturated in the solution phase for all experimental conditions, but X_{Si} was significantly reduced from 41.8% at 1 wt.% slurry density to 8.6% at 5 wt.% slurry density. The significantly reduced Si concentrations at higher slurry density conditions were likely due to the Si re-precipitation. This behavior was visibly captured in **Fig. 4(b)**, where the rapidly increased initial Si concentration was decreased with time at 5 wt.% slurry density case. The C_{Ca}/C_{Si} profiles shown in **Fig. 4(c)** also confirmed that the incongruent dissolution behaviors were enhanced with increasing the slurry density. Due to the Si re-precipitation, the C_{Ca}/C_{Si} of the dissolution of 5 wt.% hydrated cement slurry continuously increased from 3.6 to 5.3 as the dissolution progressed.

Ca and Mg leaching from alkaline solid wastes with different mineralogy via P_{CO_2} swing

As discussed earlier, one of the challenges with carbon mineralization technologies is the acid and base requirement for pH swing. The use of acid and base produced via renewable energy based electrochemical processes may ultimately address this concern as shown in **Fig. 2**. Meanwhile, there is an alternative option to perform a pH swing process for carbon mineralization, which is based on the shift of the partial pressure of CO_2 captured from different sources. A number of research groups including us have suggested this method to minimize the acid and base requirement, and have demonstrated effective dissolution of alkaline materials.[13, 34, 55, 56] The use of P_{CO_2} swing is complex since CO_2 not only provides the acidity to the CO_2-water-mineral systems but also provides carbonate ions that can react with alkaline metals to form precipitates.

The speciation of CO_2 in an aqueous phase is a strong function of pH, and thus, the dissolutions of metal oxide, metal hydroxide and metal silicates as well as the formation of solid carbonates can be significantly altered as the carbon mineralization goes through a pH swing process.

In order to provide a fundamental understanding of carbon mineralization behaviors of highly reactive alkaline solid wastes with different mineralogy via the P_{CO_2} swing, a series of dissolution and carbonation experiments were performed using Ca-rich hydrated cement, and the results of which were compared to those of Mg-rich silicate mineral (i.e., activated serpentine). First, the effect of slurry density (1 and 3 wt.%) on the hydrated cement dissolution behaviors was investigated via P_{CO_2} swing. The pH and Ca concentration profiles are given in **Fig. 5**. As expected, the pH rapidly increased right after the addition of the hydrated cement into the CO_2 saturated water (carbonic acid) and reached the maximum value (pH 8.4). This is because carbonic acid is a weak acid, while the dissolution of hydrated cement (basic material) is fast as shown in **Fig. 4**. The pH was then quickly decreased to around 6.2 and was almost constant for the rest of the experiment (**Fig. 5(a)**) as a result of the continued pH balance between CO_2 hydration and hydrated cement dissolution. Similar pH profiles were observed for activated serpentine, but the rate of pH shift was significantly slower since activated serpentine (dehydroxylated magnesium silicate) is a weaker base compared to hydrated cement.
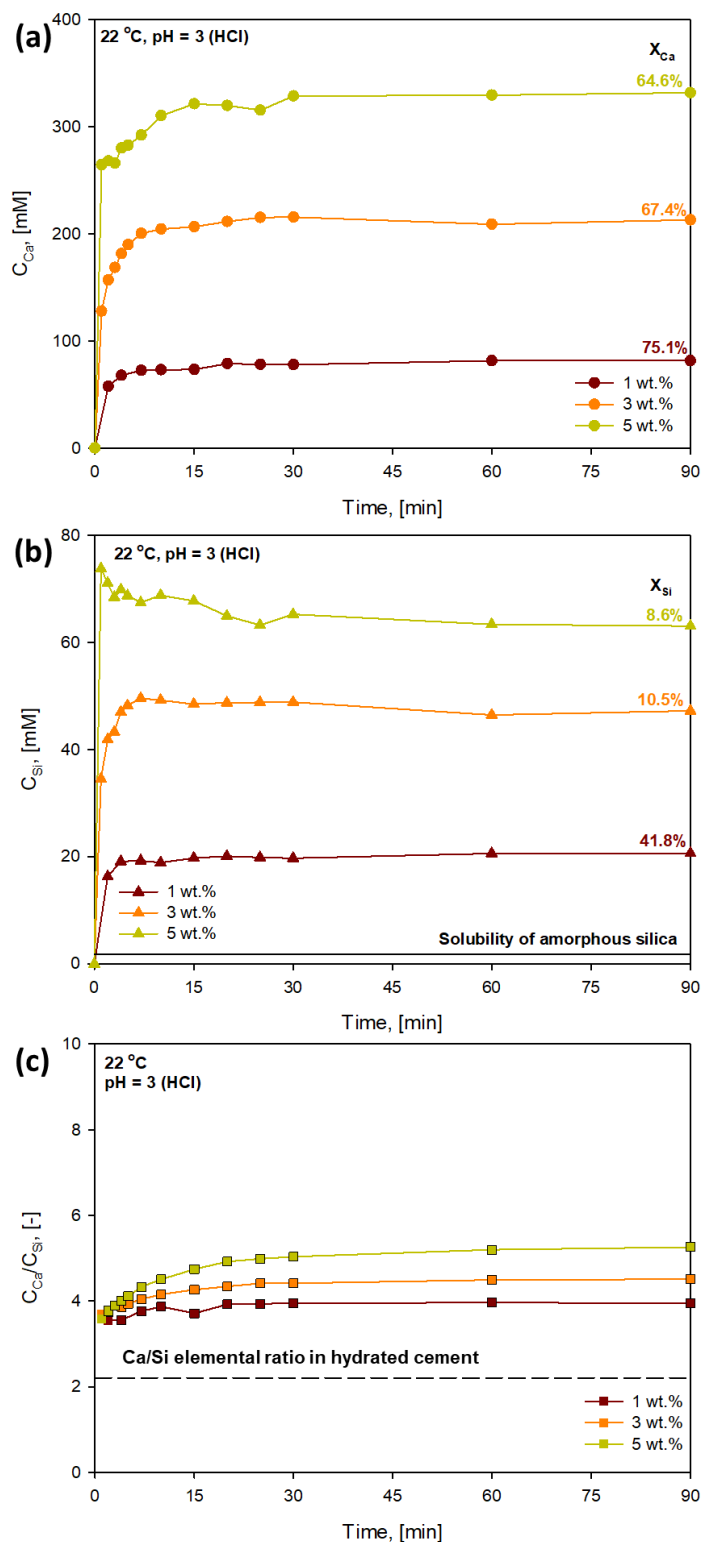
Fig. 4 Effect of slurry density on the dissolution behaviors of hydrated cement at 22 °C. (a) Ca concentration profiles; (b) Si concentration profiles; (c) Ca to Si concentration ratio profiles.
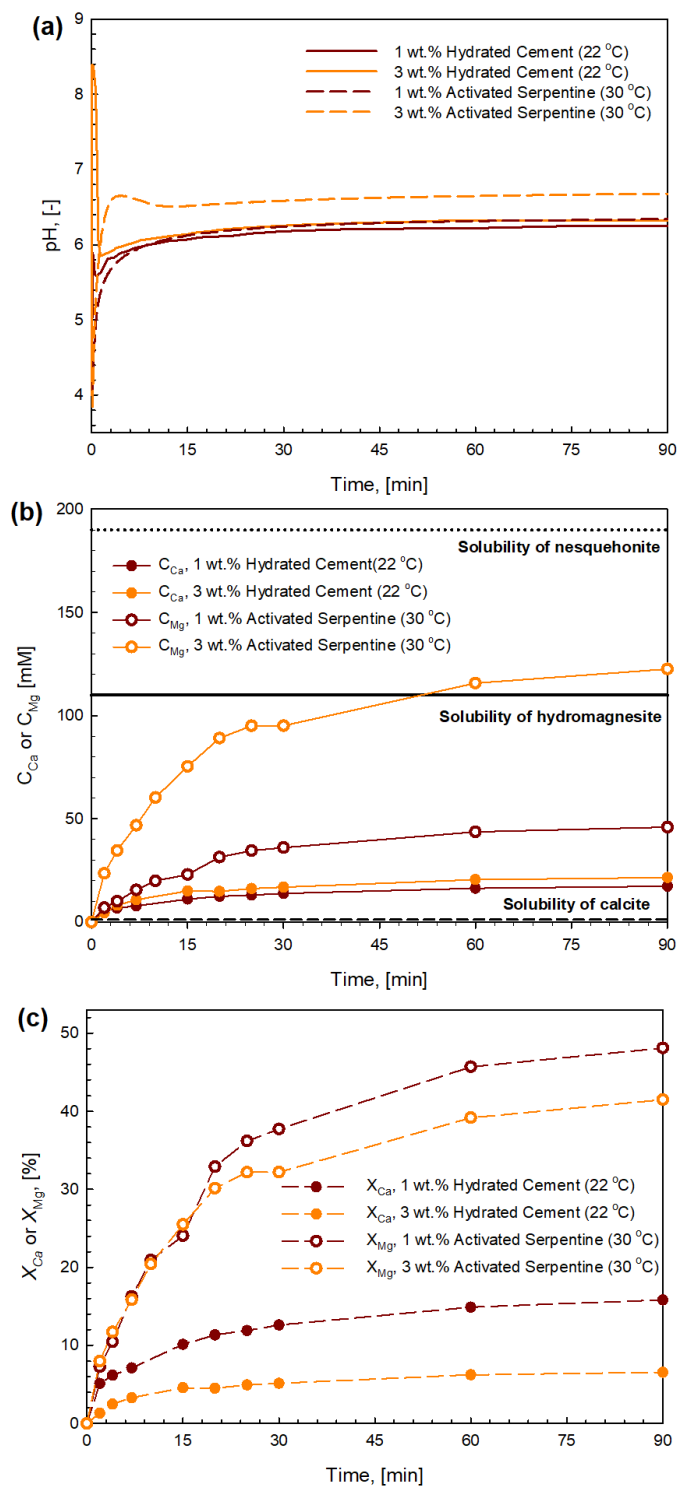
Fig. 5 Dissolution behaviors of hydrated cement and activated serpentine in the CO_2-water system (carbonic acid). (a) pH profiles, (b) Ca and Mg concentration profiles, (c) extent of Ca and Mg extraction.

Interestingly, a large difference between Ca and Mg concentrations during the dissolution of hydrated cement and activated serpentine was observed as seen in **Fig. 5(b)**. In case of activated serpentine, as high as 48.1% X_{Mg} was achieved in 90 min via P_{CO_2}. A relatively high Mg concentration of 120 mM was obtained at 3 wt.% slurry density of activated serpentine. On the other hand, during the hydrated cement dissolution experiments, the Ca concentration was maintained only at around 15 – 20 mM and the overall extent of Ca extraction was also very low (5 – 15%) even after 90 min dissolution (**Fig. 5(b)** and **5(c)**). This was unexpected since Ca-silicates are generally more soluble than Mg-silicates.

This unanticipated phenomenon of extremely low Ca concentrations in the aqueous phase was likely due to the low solubility of calcite (1.18 mM at 22 °C) at the equilibrium pH condition of the CO_2-water-hydrated cement system (about pH 6). Most of the extracted Ca was re-precipitated as a solid carbonate form ($CaCO_3$). On the other hand, Mg from activated serpentine did not precipitate as solid carbonates as illustrated in **Fig. 5(b)**. There are two Mg-carbonate phases which can be formed at the temperature range of 30 – 90 °C, nesquehonite ($MgCO_3 \cdot 3H_2O$) and hydromagnesite ($Mg_5(CO_3)_4(OH)_2 \cdot 4H_2O$).[57] Previous research has reported that nesquehonite is the most stable hydrous magnesium carbonate formed at lower temperature conditions (< 52 °C).[57-60] Thus, the upper limit of Mg extraction in the two-step P_{CO_2} swing process at 30 °C would be the solubility of nesquehonite (about 190 mM).[13] Since the Mg concentrations did not exceed the solubility limits of both Mg-carbonate phases (shown as black solid and dotted lines), the extent of Mg extraction from activated serpentine via P_{CO_2} was maintained relatively high compared to the case of hydrated cement.

These complex dissolution and precipitation processes in CO_2-water-mineral systems (minerals = e.g., hydrate concrete, activated serpentine, etc) are a strong function of pH. The

hydration and speciation of CO_2 are also greatly influenced by the solution pH. Thus, it is important to investigate solubilities of different mineral phases in CO_2-water-mineral systems as a function of pH. As shown in **Fig. 6**, calcite $(CaCO_3)$ precipitates out at alower pH conditions compared to nesquehonite $(MgCO_33H_2O)$, and the pH window of the P_{CO_2} swing turns out to be suitable for activated serpentine dissolution + nesquehonite precipitation but not adequate for hydrated cement dissolution + calcite formation. The pH of the dissolution step for hydrated cement should be lower than 5 to prevent calcite $(CaCO_3)$ precipitation during the P_{CO_2} swing process. However, due to the low acidity of carbonic acid (H_2CO_3), the pH of the hydrated cement-CO_2-water system is generally about $6 - 7$, and calcite can easily be precipitated out at this pH condition. In contrast, the synthesis of high purity precipitated magnesium carbonate (PMC) will be viable via the P_{CO_2} swing process since the solubility of nesquehonite $(MgCO_3 \cdot 3H_2O)$ is relatively high compared to calcite $(CaCO_3)$ as shown in **Fig. 6**. The formation of calcite during the hydrated cement dissolution in CO_2 saturated water was confirmed by the XRD results shown in **Fig. 7(a)**, whereas the XRD patterns of the activated serpentine after the leaching experiment did not show any Mg-carbonate (e.g. nesquehonite) peaks (**Fig. 7(b)**).
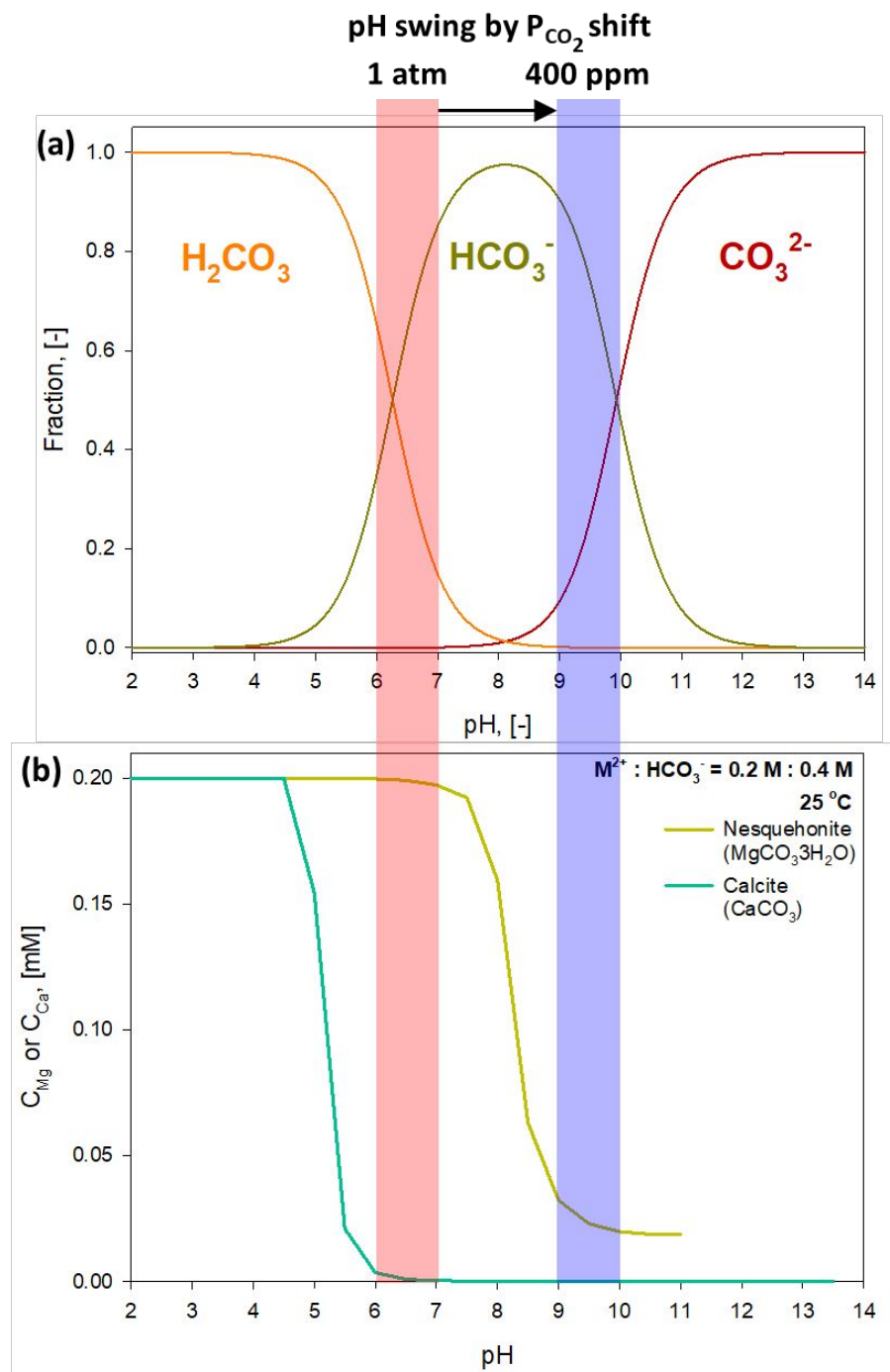
Fig. 6 Thermodynamically calculated (a) speciation of CO_2 in water and (b) solubilities of calcite ($CaCO_3$) and nesquehonite ($MgCO_3 \cdot 3H_2O$) as a function of pH. Red and blue highlighted pH conditions are associated with the dissolution and carbonation steps during a P_{CO_2} process, respectively.
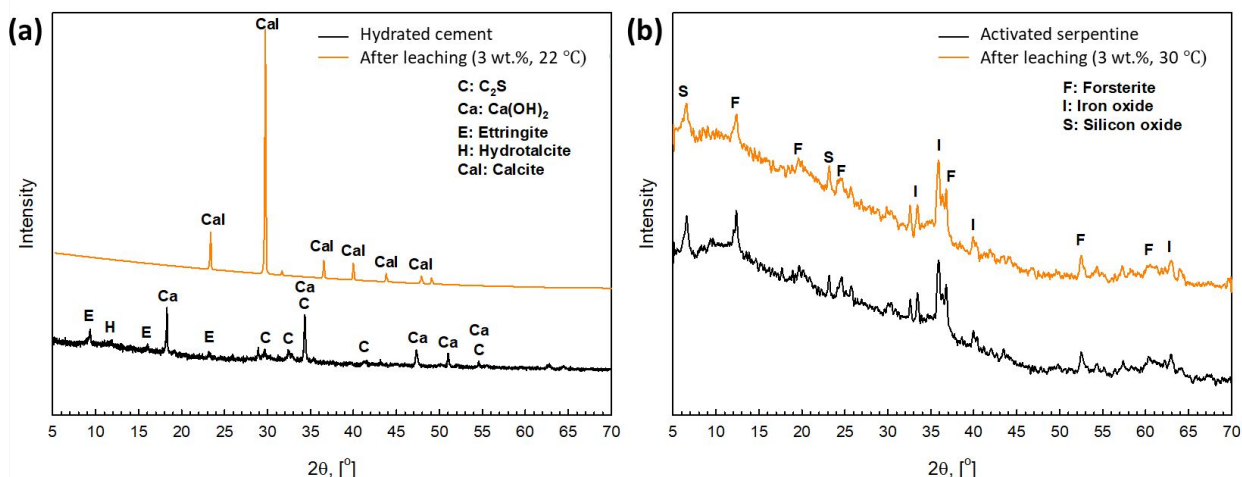
Fig. 7 X-ray diffraction patterns of (a) hydrated cement and (b) activated serpentine before and after the P_{CO_2} process.

Si phase re-precipitation during P_{CO_2} swing

Since the Ca leaching behaviors of hydrated cement changed significantly when CO_2 was used as the proton source compared to HCl, the Si dissolution and re-precipitation behaviors were also altered. As shown in **Fig. 8(a)** and **8(b)**, a rapid increase in Si concentration was observed at the beginning of the mineral dissolution for both hydrated cement and activated serpentine, respectively. The supersaturation of amorphous silica was significantly greater for activated serpentine due to the presence of more Si; activated serpentine contains 20.5 wt.% Si, whereas hydrated cement only contains 14.0 wt.% Si. When the Si extraction rate was overtaken by the Si precipitation rate, the Si concentration started to decrease towards the solubility limit of amorphous silica indicating the re-precipitation of extracted Si. The slurry density may have also influenced the Si re-precipitation behaviors since a large number of nuclei (mineral particles) and a larger surface area at high slurry density conditions would have accelerated the Si re-precipitation kinetics.[13, 61]
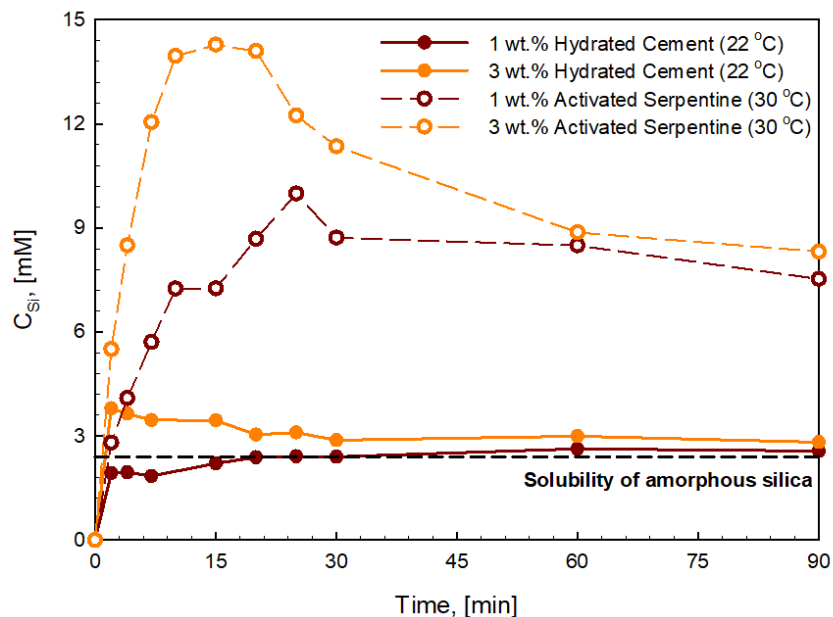
Fig. 8 Si concentration profiles of hydrated cement-CO_2-water system and active serpentine-CO_2-water system with 1 wt. % and 3 wt.% slurry densities at 22-30 °C.

These results indicate that significant re-precipitation of extracted Si would have resulted in the formation of a thicker Si-rich passivation layer on the activated serpentine particle surface under higher slurry density conditions. Therefore, the reduced extent of Mg extraction (X_{Mg}) with increasing slurry density shown in **Fig. 5(c)** would be also attributed to the formation of a thicker Si-rich passivation layer. To overcome the severe passivation effect and enhance the Mg extraction behavior of the activated serpentine at higher slurry density conditions, a proper activation method to minimize the mass transfer limitation would be required. Researchers including our group have suggested mechanical abrasion to remove the passivation layer and showed the greatly enhanced Mg extraction kinetics.[32, 51, 62] These physical approaches may also be able to enhance the dissolution of hydrated cement, but its higher reactivity compared to natural silicate minerals may lead to different transition behaviors from surface reaction limited to mass transfer limited reaction regimes.

2

Molecular level study on leaching behaviors of different silicate structures of alkaline solid wastes

As illustrated in this study, there is a strong relationship between the fates of Ca/Mg and Si phases in alkaline solid wastes including hydrated cement. In particular, the structures of Si phases change throughout the carbon mineralization process, since it undergoes dissolution and re-precipitation reactions. Thus, it is important to understand the structure of Si phases in order to better design carbon mineralization technologies for alkaline solid wastes.

The Ca and Mg-bearing silicate materials from industrial waste streams and nature react with CO_2 via the following two steps: 1) leaching of metal ions from silicates by an ion-exchange reaction between H^+ and M^{n+} (e.g., M = Ca or Mg), 2) precipitation of extracted metal ions by reacting with dissolved CO_2 (CO_3^{2-} ion). Between these two steps, the dissolution reaction is often the rate-determining step due to the relatively high activation energy of the surface dissolution reaction of silicate materials.[36] The activation energy is related to the chemical stability and the structure of the silicate materials. Therefore, investigating the silicate materials' structure at the molecular level is essential to understand the Ca and Mg leaching behaviors.[63]

The SiO_4 tetrahedra structures are generally denoted as Q^n (n = 0, 1, 2, 3, 4), where n indicates the number of shared oxygens that bridge silicon to other SiO_4 tetrahedra. **Table 2** shows the various silicate structures and their characteristic peaks that can be determined by the ^{29}Si MAS NMR technique. In this study, the silicate structural changes in hydrated cement and activated serpentine before and after their dissolution were investigated using ^{29}Si NMR. As shown in **Fig. 9(a)**, the raw hydrated cement has mostly Q^1 (-81 ppm) structure. The peak near -81 ppm is consistent with a similar signature for hydrated OPC and tricalcium silicate,[64, 65] and is assigned to the terminal silicate tetrahedral structural unit, Q^1. Lineshape simulation suggests that roughly 20% of the total resonance includes unresolved smaller components near -72 ppm and -93 ppm. These

features are consistent with the isolated Q^0 signature of OPC and a small amount of the fully linked $Q^4(3Al)$, a signature of kaolinite,[66] respectively. After the acid leaching for 24 hr, the dominant peak was changed to the one near -100 ppm (Q^4) due to the fully linked tetrahedral SiO_2 structure. The line width for the hydrated cement residue after the dissolution, being twice as large as the raw material, is consistent with a larger distribution of bond angles and greater heterogeneity among silicate sites, while a higher crystalline content seems to be the case in the untreated hydrated cement. The simulation indicates that roughly 10% of the signal intensity is centered near -85 ppm; indicating a likely association with unresolved Q^1 and Q^2 silicate structures.

In the case of activated serpentine, the recent study has revealed that it is a mixture of Q^0, Q^1, Q^2 Q^3, and Q^4 silicate structures (**Fig. 9(b)**).[63] After acid leaching of activated serpentine, the Q^0 – Q^3 silicate structures were almost digested and the residue contained mostly hydrated amorphous silica (Q^3 $((SiO)_3SiOH)$, -102.1 ppm, and Q^4 $((SiO)_4Si)$, -113.3 ppm)[67, 68] with a minor quantity of undissolved Q^3 structure (-92.9 ppm).[63]
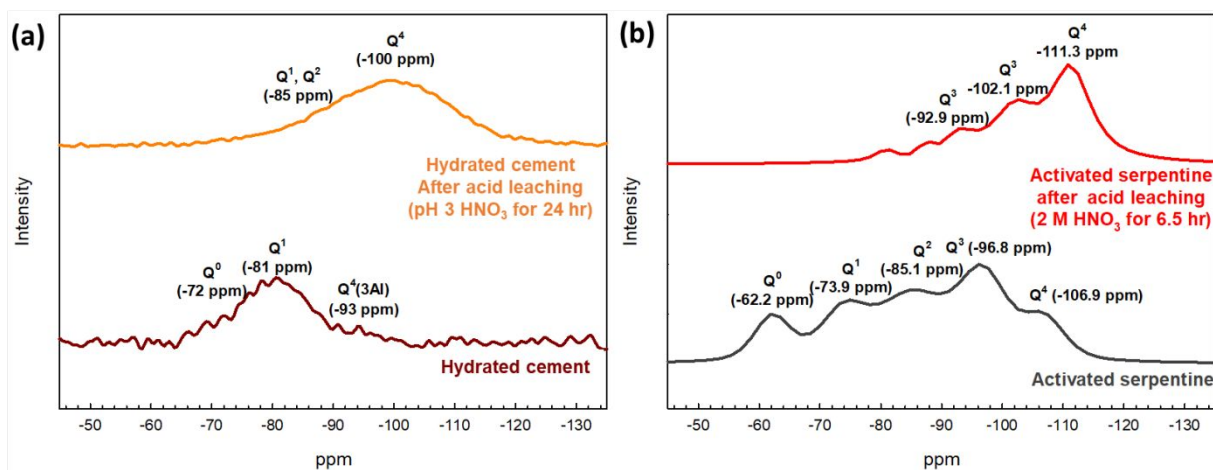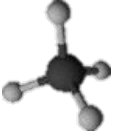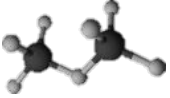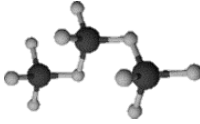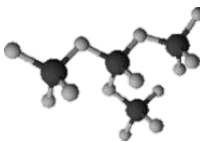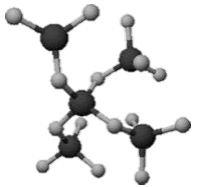

Fig. 9 ^{29}Si MAS NMR spectra of **(a)** hydrated cement and **(b)** activated serpentine (adapted from [63]) before and after dissolution.

Table 2. ^{29}Si chemical shifts of various silicate structures (adapted from Rim et al., 2020)[63]

	Structure	Compound	Chemical Shift (ppm)	References
Q⁰		monticellite (CaMgSiO₄) chondrodite (Mg₅[SiO₄]₂(OH,F)₂) forsterite (Mg₂SiO₄) olivine ((Mg,Fe)₂SiO₄)	-66 -60 -61.9 -62	Smith et al.[69] Mägi et al.[70] Mägi et al.[70] Mägi et al.[70]
Q¹		akermanite (Ca₂MgSi₂O₇) rankinite (Ca₃Si₂O₇)	-73 -74.5	Smith et al.[69] Mägi et al.[70]
Q²		clinoenstatite (MgSiO₃) orthoenstatite (MgSiO₃) diopside (CaMgSi₂O₆) fibrous tremolite (Ca₂Mg₅[Si₄O₁₁]₂(OH)₂) wollastonite (CaSiO₃)	-81; -83 -82 -84 -87.8; -92.2 -89	Smith et al.[69] Mägi et al.[70] Mägi et al.[70] Mägi et al.[70] Hansen et al.[71]
Q³		datolite (CaBSiO₄(OH)) serpentine (Mg₃(Si₂O₅)(OH)₄) talc (Mg₃(Si₄O₁₀)(OH)₂) sepiolite (Mg₄Si₆O₁₅(OH)₂·2H₂O)	-96 -94 -98.1 -92; -95; -98	Smith et al.[69] Mägi et al.[70] Mägi et al.[70] Barron et al.[72]
Q⁴		quartz (SiO₂) coestite (SiO₂) crystobalite (SiO₂) tridymite (SiO₂) silicalite (SiO₂) holdstite (SiO₂) silica gel hydrous α-silica	-108 -108.1; 113.9 -108.5 -109.3 - -114 -109.9 - -117 -108.9; -115; -119.4 -91 (Q²); -101 (Q³); -110 -92.1 (Q²); -101.6 (Q³); -111.1	Smith et al.[69] Smith & Blackwell[73] Smith & Blackwell[73] Smith & Blackwell[73] Fyfe et al.[74] Smith & Blackwell[73] Leonardelli et al.[67] Chemtob et al.[68]

Precipitation of Calcium Carbonates (PCC) via pH swing

In order to synthesize high purity PCC from the hydrated cement, a two-step pH swing process was carried out as described in the Materials and Method section. The dissolution of the hydrated cement was done under a fixed pH of 3, and the resulting slurry was filtered to separate out solid residues. The Ca-rich leachate was then transferred to a reactor, where the pH of the leachate was increased to 9 by dropwise adding 20 ml of 50 wt.% NaOH solution. Next, CO_2 gas was bubbled into the reactor at a rate of 30 ml/min until the completion of the carbonation reaction, which was denoted by the reduced Ca concentration in the solution phase. Two reaction temperatures were investigated, 30 °C and 60 °C. The resulting slurry was filtered to separate the precipitated calcium carbonates (PCC) and the produced PCC was washed with D.I. water prior to the analyses by a series of characterization methods including TGA, XRD, and SEM.

The crystal structure of the PCC was determined using XRD with 2θ values between 5° to 70°. The refinement of XRD was performed by applying the Reitveld refinement method and MAUD software. Calcium carbonate has three anhydrous polymorphs: calcite, aragonite, and vaterite.[75] Calcite is the most common and stable phase of $CaCO_3$, exhibiting a rhomboidal crystalline structure. It is a naturally occurring phase that is extensively present in rocks, such as limestone, marble, etc. Aragonite is the second most stable phase of calcium carbonate, having a needle or rod-like morphology. It commonly coexists with calcite in nature and is formed through precipitation from seawater or mineral spring environments. Aragonite tends to convert to calcite at ambient temperature and pressure over a relatively long period (a few decades).[75] Spherical vaterite is the most unstable polymorph of calcium carbonate at ambient conditions and has a much higher solubility than the other two polymorphs. As such, it does not commonly exist in nature. When exposed to water, it transforms to calcite at ambient temperature or aragonite at high temperatures within a relatively short time (a few hours to some days).[75] As shown in **Fig. 10(a)**,

the major peaks of the solid products corresponded to the calcite polymorph, and there was no presence of vaterite or aragonite. This was expected since the carbonation reaction was performed at relatively lower reaction temperatures of 30 °C and 60 °C. Further, the SEM image also shows cubic structures confirming the formation of calcite (**Fig. 10(b)**).
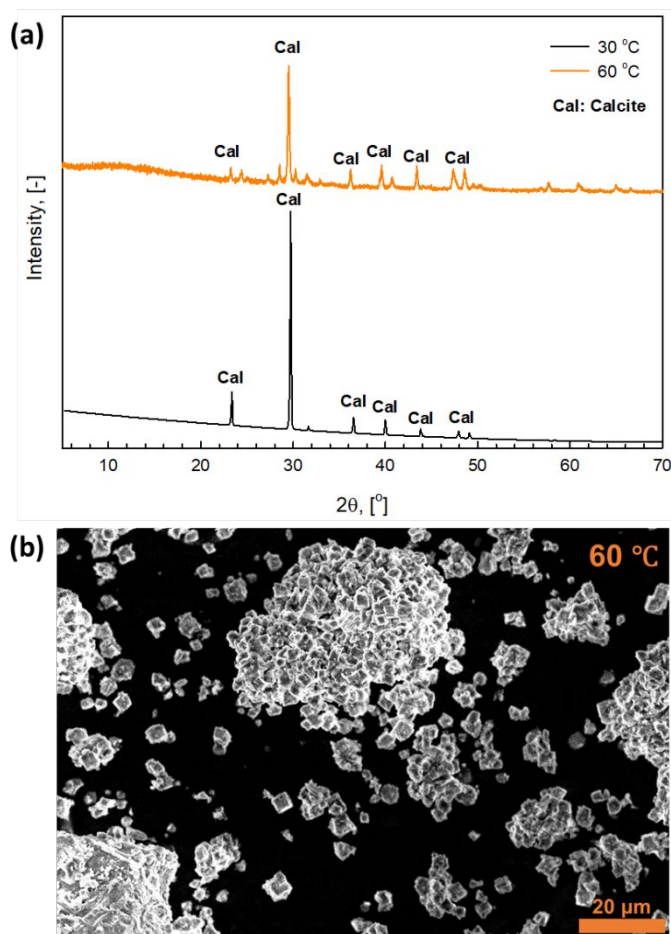

Fig. 10 Characterization of Precipitated Calcium Carbonate (PCC) derived from the dissolution and carbonation of hydrated cement. **(a)** X-ray diffraction (XRD) spectra and **(b)** Scanning electron microscope (SEM) of PCC.

Hydration behaviors of cement incorporated with precipitated calcium carbonate

Finally, the PCC (calcite) synthesized from the hydrated cement, which is the reactive and highest carbon footprint component of waste concrete, was tested for its performance as a

substitution for the OPC to prepare new construction materials. The calorimetric results of cement with different amounts of incorporated PCC (10 – 30 wt.%) are presented in terms of the heat flow and cumulative heat release during the curing process. As shown in **Fig. 11**, the heat flow curve of conventional OPC has two main peaks that correspond to the reaction of silicate (C_3S) and aluminate (C_3A), respectively, as denoted in **Fig. 11(a)**.[76] The addition of PCC primarily composed of calcite increased the intensity of these two peaks. This indicates that the presence of calcium carbonate was able to accelerate the reactions of these two cement clinker phases - silicate (C_3S) and aluminate (C_3A). The higher the replacement level, the stronger the accelerating effect was. This finding is consistent with the results in the literature.[77, 78]
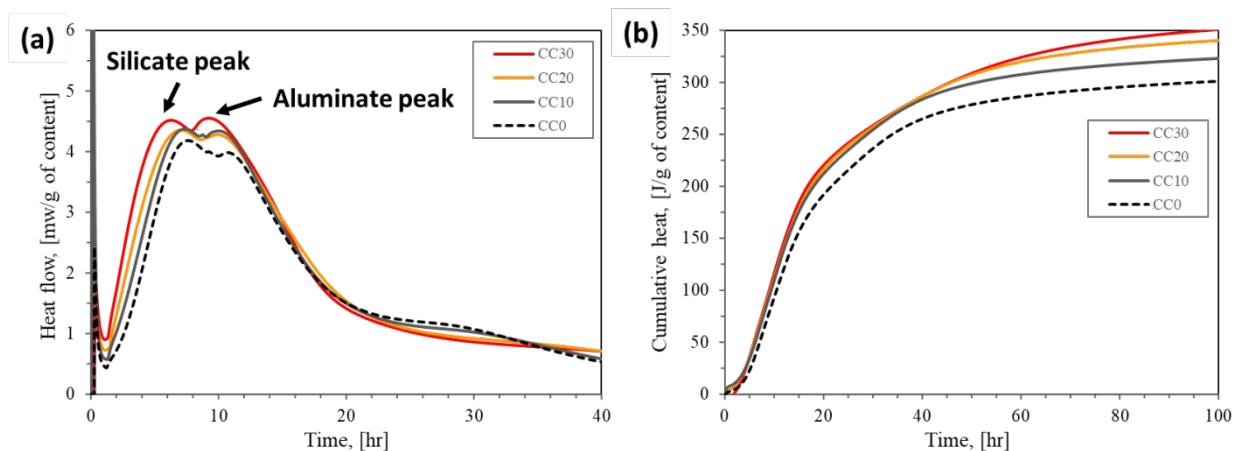

Fig. 11 Hydration behaviors of cement pastes containing different amounts of calcite (0-30 wt.%) produced from waste concrete as a replacement of Ordinary Portland Cement (OPC). **(a)** Heat flow and **(b)** cumulative heat release of cement paste during the curing process.

The mechanisms of the acceleration of C_3S and C_3A can be different: the former was mainly because of the physical presence of calcite, which provided more nucleation sites for the growth of hydrated cement phases, while the latter was perhaps due to the reaction between calcite and aluminate, forming mono- and hemi-carboaluminates.[79] Such acceleration can be beneficial for the properties of the produced concrete, as it can offset the dilution of the cementitious system due to

cement substitution, particularly at early ages. The cumulative heat release presented in **Fig. 11(b)** also indicated a higher hydration degree of cement for all samples incorporating calcium carbonates up to an age of 4 days (96 hours).

CO_2 utilization and sequestration potential in built environment via upcycling of waste concrete

The construction industry is one of the most carbon intensive industries. According to a recent report, about 38% of the total carbon emissions can be attributed to the built environment comprising of building operations, both residential and commercial, and building materials (see **Fig. 12**).[80] As the population and urbanization rates increase, the construction industry will grow in tandem, with the global growth in this sector projected to be about 67% by 2050.[81] This leads to an increasing interest and need in applying Carbon Capture, Utilization and Storage (CCUS) technologies in built environment.
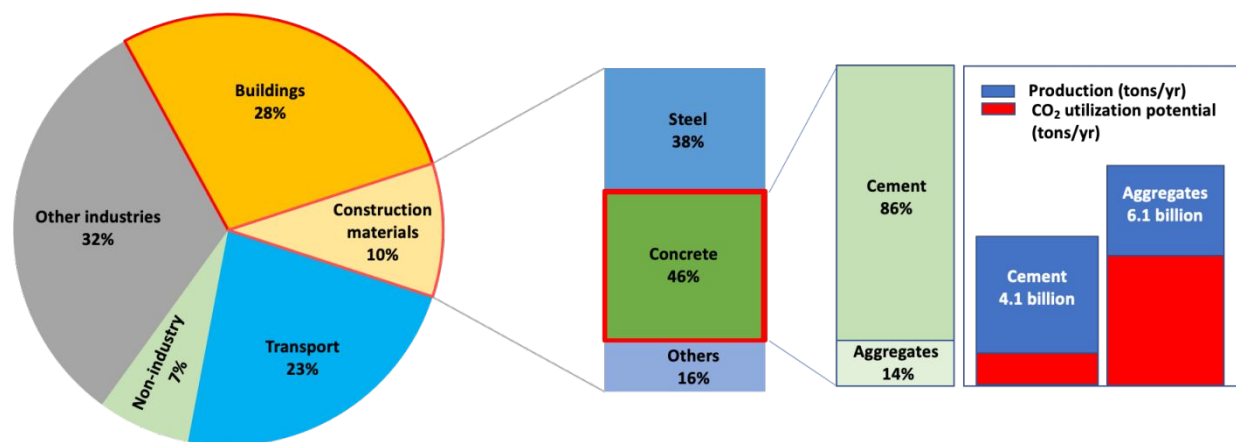

Fig. 12 CO_2 emission by sectors and materials in 2020.[82-84]

Among the construction materials, concrete is known to have the highest carbon footprint, about 150 kg CO_2 eq. / ton of concrete.[80] Due to its massive production worldwide, concrete contributes to about 8% of the total CO_2 emissions in the industrial sectors.[80] The main component responsible for the large carbon emission is the calcination of limestone in a clinker producing

cementitious materials, which corresponds to about 866 kg CO_2 eq. / ton of cement.[80] Both indirect

CO_2 emissions required for providing heat to the clinker reaction occuring at 1400 °C and direct

CO_2 release as a byproduct of the calcination reaction of limestone and clay are counted towards

the carbon intensity of cement and concrete. About 50% of the carbon emissions from the cement

manufacturing process are direct emissions, 45% are energy-driven and about 5% is related to

transportation and handling of the materials.[85, 86]

The rapid rate of infrastructure growth forces demolition rates to go hand in hand with

increasing construction rates.[87] Due to evolving needs and reduced service life, some trends point

towards an average lifespan of 20-50 years for a building.[87] This leads to a vast amount of

construction and demolition waste (C&DW) being generated. The global C&DW exceed 3 billion

tons per year as of 2018.[88] Munaro et al.[89] provided a comprehensive review on built environment

research and the role of circular economy in it with a focus on policies. Since the 1970s, this

concept of a circular economy has slowly been gaining attention due to the limited disposal options

for the large volume of C&DW.[89] The common method of disposing municipal waste is

incineration, but this cannot be done for construction and demolition wastes due to thermal

inertness up to 1200 °C. Further, it cannot be broken down by aerobic or anaerobic microbes.[90]

The most common disposal method remains to be landfills; about 24% of the global C&DW is

currently landfilled.[91] Some waste concrete are used as aggregates and incorporated into other

manufacturing industries.[91] According to a recent report by U.S. Environmental Protection

Agency, 67% of all C&DW is concrete and in 2018, 71.2 million tons of concrete was landfilled.[91]

In regards to carbon storage, $5.7 - 57\%$ CO_2 from concrete manufacturing can be reabsorbed

throughout the lifetime of buildings, albeit dependent on the type of concrete, exposure time and,

production conditions.[92] Researchers have attempted to mimic this thermodynamically favorable

phenomenon of mineral weathering to produce value-added calcium carbonates from waste concrete under controlled reaction environments to allow maximum conversions.[92] An active research area in this field is the carbonation of recycled aggregates, which turns the residual mortar on the recycled aggregates into calcium carbonate. The carbonated recycled aggregates are incorporated into concrete, and they have been reported to enhance the properties of the concrete compared to untreated recycled aggregates.[93-95] In light of this, the dissolution and carbonation processes of hydrated cement developed in this study have a great potential to produce new construction materials with reduced carbon intensity, while minimizing landfills of wastes.

Conclusions

In this study, the dissolution and carbonation behaviors of hydrated cement was investigated in order to develop a CO_2 utilization technology that can reduce or even close the calcium and carbon cycles in the built environment. Two solvent systems – one using a strong acid (HCl at pH 3) produced using renewable energy and the other using carbonic acid produced by dissolving captured CO_2 into water – were investigated for the fundamental understanding of the two-step pH swing carbon mineralization process. Specifically, the effects of temperature and slurry density on the elemental (Ca/Mg and Si) extraction from the hydrated cement and activated serpentine were studied for far-from-equilibrium and near equilibrium conditions. Non-stoichiometric leaching behaviors (between Ca and Si) of hydrated cement were observed, and the re-precipitation of Si phases was correlated to the mass transfer limitations during mineral dissolutions. It was found that unlike Mg-silicate minerals, the dissolution of hydrated cement cannot be achieved via P_{CO_2} swing alone because of the low solubility of calcite ($CaCO_3$) under the pH conditions created by bubbling CO_2. The bubbling of CO_2 into cement slurry would result in Ca leaching directly followed by in-situ formation of calcite, but the purity of the produce calcite would be lower than

that of PCC produced via a two-step pH swing process. The incorporation of PCC derived from

waste concrete into new cement pastes as a replacement of OPC resulted in improved hydration

behaviors, and suggested that waste concrete can be upcycled to produce sustainable construction

materials via CO_2 utilization.

ACKNOWLEDGMENT

References

1.   *Intergovernmental Panel on Climate Change, (IPCC), Foruth Assessment Report, Working Group
      III, IPCC, Geneva, Switzerland*, 2007.

2.   E. J. Swanson, K. J. Fricker, M. Sun and A.-H. A. Park, *Physical Chemistry Chemical Physics*, 2014, **16**, 23440-23450.

3.   K. J. Fricker and A.-H. A. Park, *Industrial & Engineering Chemistry Research*, 2014, **53**, 18170-18179.

4.   H. Zhao, N. Dadap and A.-H. A. Park, *Fluidization XIII: New Paradigm in Fluidization Engineering; Kim, S. D.; Kong, Y.; Lee, J. K.; Seo, Y. C., Eds.; Engineering*, 2010, **Conferences International: New York**, 821– 828.

5.   K. S. Lackner and H. Ziock, *Mod. Power Syst.*, 2000, **20**, 31-32.

6.   L. C. Pasquier, G. Mercier, J. F. Blais, E. Cecchi and S. Kentish, *Environ Sci Technol*, 2014, **48**, 5163-5170.

7.   R. D. Balucan, B. Z. Dlugogorski, E. M. Kennedy, I. V. Belova and G. E. Murch, *Int J Greenh Gas Con*, 2013, **17**, 225-239.

8.   R. D. Balucan, E. M. Kennedy, J. F. Mackie and B. Z. Dlugogorski, *Greenhouse Gases: Science and Technology*, 2011, **1**, 294-304.

9.   B. Z. Dlugogorski and R. D. Balucan, *Renewable and Sustainable Energy Reviews*, 2014, **31**, 353-367.

10.   C. Du Breuil, L. Cesar-Pasquier, G. Dipple, J. F. Blais, M. C. Iliuta and G. Mercier, *Minerals-Basel*, 2019, **9**.

11.   J. J. Li and M. Hitch, *Int Biodeter Biodegr*, 2018, **128**, 63-71.

12.   P. Raschman, A. Fedorockova and G. Sucik, *Hydrometallurgy*, 2013, **139**, 149-153.

13.   M. Werner, S. Hariharan and M. Mazzotti, *Physical Chemistry Chemical Physics*, 2014, **16**, 24978-24993.

14.   G. Gadikota and A. H. A. Park, *Carbon Dioxide Utilisation: Closing the Carbon Cycle, 1st Edition*, 2015, DOI: 10.1016/B978-0-444-62746-9.00008-6, 115-137.

15.   K. J. Fricker and A.-H. A. Park, *Chemical Engineering Science*, 2013, **100**, 332-341.

16.   G. Gadikota, C. Natali, C. Boschi and A.-H. A. Park, *Journal of Hazardous Materials*, 2014, **264**, 42-52.

17.   G. Gadikota, J. Matter, P. Kelemen, P. V. Brady and A.-H. A. Park, *Fuel*, 2020, **277**, 117900.

18.   S. Hong, H. D. Huang, G. Rim, Y. Park and A.-H. A. Park, *ACS Sustainable Chemistry & Engineering*, 2020, **8**, 18519-18527.

19.   *Report of the Mission Innovation Carbon Capture, Utilization, and Storage Expert's Workshop*, September 26-28, 2017.

20.   E. National Academies of Sciences, and Medicine, *DC: The National Academies Press*, 2019, **Gaseous Carbon Waste Streams Utilization: Status and Research Needs**.

21.   P. Renforth, C. L. Washbourne, J. Taylder and D. A. C. Manning, *Environ Sci Technol*, 2011, **45**, 2035-2041.

22.   S.-Y. Pan, T.-C. Ling, A.-H. A. Park and P.-C. Chiang, *Aerosol and Air Quality Research*, 2018, **18**, 829-848.

23.   G. Gadikota, E. J. Swanson, H. Zhao and A.-H. A. Park, *Industrial & Engineering Chemistry Research*, 2014, **53**, 6664-6676.

24.   G. Gadikota, J. Matter, P. Kelemen and A.-h. A. Park, *Physical Chemistry Chemical Physics*, 2014, **16**, 4679-4693.

25.   H. Zhao, Y. Park, D. H. Lee and A.-H. A. Park, *Physical Chemistry Chemical Physics*, 2013, **15**, 15185-15192.

26.   N. Zhang, H. Duan, T. R. Miller, V. W. Y. Tam, G. Liu and J. Zuo, *Renewable and Sustainable Energy Reviews*, 2020, **117**, 109495.

27.   A. Sanna, M. Uibu, G. Caramanna, R. Kuusik and M. M. Maroto-Valer, *Chemical Society Reviews*, 2014, **43**, 8049-8080.

28. H. Xie, L. Tang, Y. Wang, T. Liu, Z. Hou, J. Wang, T. Wang, W. Jiang and P. Were, *Environmental Earth Sciences*, 2016, **75**, 615.

29. T. A. Branca, V. Colla, D. Algermissen, H. Granbom, U. Martini, A. Morillon, R. Pietruck and S. Rosendahl, *Metals*, 2020, **10**.

30. Carbon dioxide emissions from energy consumption in the U.S. from 1975 to 2019 (in million metric tons of carbon dioxide), DOI: https://www.statista.com/statistics/183943/us-carbon-dioxide-emissions-from-1999/).

31. G. Gadikota, K. Fricker, S.-H. Jang and A.-H. A. Park, in *Advances in CO$_2$ Capture, Sequestration, and Conversion*, American Chemical Society, 2015, vol. 1194, ch. 12, pp. 295-322.

32. A. H. A. Park and L. S. Fan, *Chemical Engineering Science*, 2004, **59**, 5241-5247.

33. A.-H. A. Park, R. Jadhav and L.-S. Fan, *The Canadian Journal of Chemical Engineering*, 2003, **81**, 885-890.

34. S. Hariharan and M. Mazzotti, *Chem Eng J*, 2017, **324**, 397-413.

35. T. K. Oliver, F. Farhang, T. W. Hodgins, M. S. Rayson, G. F. Brent, T. S. Molloy, M. Stockenhuber and E. M. Kennedy, *Energ Fuel*, 2019, **33**, 1753-1766.

36. A. A. Olajire, *J Petrol Sci Eng*, 2013, **109**, 364-392.

37. M. Herrero-Gonzalez, P. Diaz-Guridi, A. Dominguez-Ramos, A. Irabien and R. Ibañez, *Separation and Purification Technology*, 2020, **242**, 116785.

38. M. Reig, S. Casas, C. Valderrama, O. Gibert and J. L. Cortina, *Desalination*, 2016, **398**, 87-97.

39. M. Wang, K.-k. Wang, Y.-x. Jia and Q.-c. Ren, *Journal of Membrane Science*, 2014, **452**, 54-61.

40. K. Ghyselbrecht, A. Silva, B. Van der Bruggen, K. Boussu, B. Meesschaert and L. Pinoy, *Journal of Environmental Management*, 2014, **140**, 69-75.

41. K. Ghyselbrecht, M. Huygebaert, B. Van der Bruggen, R. Ballet, B. Meesschaert and L. Pinoy, *Desalination*, 2013, **318**, 9-18.

42. M. Sanger, B. M. Natarajan, B. Wang, T. Edil and M. Ginder-Vogel, *Journal of Hazardous Materials*, 2020, **385**, 121562.

43. W. H. Casey, H. R. Westrich, J. F. Banfield, G. Ferruzzi and G. W. Arnold, *Nature*, 1993, **366**, 253-256.

44. H. Bearat, M. J. McKelvy, A. V. G. Chizmeshya, D. Gormley, R. Nunez, R. W. Carpenter, K. Squires and G. H. Wolf, *Environ Sci Technol*, 2006, **40**, 4802-4808.

45. O. S. Pokrovsky and J. Schott, *Geochim Cosmochim Ac*, 2000, **64**, 3313-3325.

46. O. S. Pokrovsky and J. Schott, *Geochim Cosmochim Ac*, 2000, **64**, 3299-3312.

47. D. Daval, O. Sissmann, N. Menguy, G. D. Saldi, F. Guyot, I. Martinez, J. Corvisier, B. Garcia, I. Machouk, K. G. Knauss and R. Hellmann, *Chem Geol*, 2011, **284**, 193-209.

48. N. C. Johnson, B. Thomas, K. Maher, R. J. Rosenbauer, D. Bird and G. E. Brown, *Chem Geol*, 2014, **373**, 93-105.

49. F. Wang, D. Dreisinger, M. Jarvis and T. Hitchins, *Miner Eng*, 2019, **131**, 185-197.

50. F. Wang, D. Dreisinger, M. Jarvis, T. Hitchins and D. Dyson, *Chem Eng J*, 2019, **360**, 452-463.

51. G. Rim, D. Wang, M. Rayson, G. Brent and A.-H. A. Park, *Industrial & Engineering Chemistry Research*, 2020, **59**, 6517–6531.

52. F. Farhang, T. K. Oliver, M. S. Rayson, G. F. Brent, T. S. Molloy, M. Stockenhuber and E. M. Kennedy, *J Co2 Util*, 2019, **30**, 123-129.

53. E. Benhelal, T. K. Oliver, F. Farhang, J. M. Hook, M. S. Rayson, G. F. Brent, M. Stockenhuber and E. M. Kennedy, *Industrial & Engineering Chemistry Research*, 2019, DOI: 10.1021/acs.iecr.9b04379.

54. R. Hellmann, R. Wirth, D. Daval, J. P. Barnes, J. M. Penisson, D. Tisserand, T. Epicier, B. Florin and R. L. Hervig, *Chem Geol*, 2012, **294**, 203-216.

55. S. Hariharan and M. Mazzotti, *Crystal Growth & Design*, 2017, **17**, 317-327.

56. T. K. Oliver, B. Z. Dlugogorski and E. M. Kennedy, *Miner Eng*, 2014, **61**, 113-120.

57.   P. J. Davies and B. B., *Chem Geol*, 1973, **12**, 289-300.
58.   P. Ballirano, C. De Vito, V. Ferrini and S. Mignardi, *Journal of Hazardous Materials*, 2010, **178**, 522-528.
59.   V. Ferrini, C. De Vito and S. Mignardi, *Journal of Hazardous Materials*, 2009, **168**, 832-837.
60.   J. T. Kloprogge, W. N. Martens, L. Nothdurft, L. V. Duong and G. E. Webb, *J Mater Sci Lett*, 2003, **22**, 825-829.
61.   F. Farhang, M. Rayson, G. Brent, T. Hodgins, M. Stockenhuber and E. Kennedy, *Chem Eng J*, 2017, **330**, 1174-1186.
62.   M. I. Rashid, E. Benhelal, F. Farhang, T. K. Oliver, M. S. Rayson, G. F. Brent, M. Stockenhuber and E. M. Kennedy, *J Clean Prod*, 2019, **212**, 151-161.
63.   G. Rim, A. K. Marchese, P. Stallworth, S. G. Greenbaum and A.-H. A. Park, *Chem Eng J*, 2020, **396**, 125204.
64.   M. D. Andersen, H. J. Jakobsen and J. Skibsted, *Cement and Concrete Research*, 2006, **36**, 3-17.
65.   A. Mendes, W. P. Gates, J. G. Sanjayan and F. Collins, *Materials and Structures*, 2011, **44**, 1773-1791.
66.   M. R. Rowles, J. V. Hanna, K. J. Pike, M. E. Smith and B. H. O'Connor, *Applied Magnetic Resonance*, 2007, **32**, 663.
67.   S. Leonardelli, L. Facchini, C. Fretigny, P. Tougne and A. P. Legrand, *Journal of the American Chemical Society*, 1992, **114**, 6412-6418.
68.   S. M. Chemtob, G. R. Rossman and J. F. Stebbins, *Am Mineral*, 2012, **97**, 203-211.
69.   K. A. Smith, R. J. Kirkpatrick, E. Oldfield and D. M. Henderson, *Am Mineral*, 1983, **68**, 1206-1215.
70.   M. Magi, E. Lippmaa, A. Samoson, G. Engelhardt and A. R. Grimmer, *J Phys Chem-Us*, 1984, **88**, 1518-1522.
71.   M. R. Hansen, H. J. Jakobsen and J. Skibsted, *Inorg Chem*, 2003, **42**, 2368-2377.
72.   P. F. Barron, P. Slade and R. L. Frost, *J Phys Chem-Us*, 1985, **89**, 3305-3310.
73.   J. V. Smith and C. S. Blackwell, *Nature*, 1983, **303**, 223-225.
74.   C. A. Fyfe, G. C. Gobbi, J. Klinowski, J. M. Thomas and S. Ramdas, *Nature*, 1982, **296**, 530-533.
75.   B. Jones, *Sedimentary Geology*, 2017, **353**, 64-75.
76.   J. W. Bullard, H. M. Jennings, R. A. Livingston, A. Nonat, G. W. Scherer, J. S. Schweitzer, K. L. Scrivener and J. J. Thomas, *Cement and Concrete Research*, 2011, **41**, 1208-1223.
77.   A. Kumar, T. Oey, G. Falzone, J. Huang, M. Bauchy, M. Balonis, N. Neithalath, J. Bullard and G. Sant, *Journal of the American Ceramic Society*, 2017, **100**, 3316-3328.
78.   T. Oey, A. Kumar, J. W. Bullard, N. Neithalath and G. Sant, *Journal of the American Ceramic Society*, 2013, **96**, 1978-1990.
79.   B. Lothenbach, G. Le Saout, E. Gallucci and K. Scrivener, *Cement and Concrete Research*, 2008, **38**, 848-860.
80.   O. R. Ian Hamilton, *United Nations Environment Programme*, 2020.
81.   N. C. Onat and M. Kucukvar, *Renewable and Sustainable Energy Reviews*, 2020, **124**, 109783.
82.   IEA, *World Energy Balances 2020 EDITION DATABASE DOCUMENTATION*, 2020.
83.   IEA, *Energy Technology Perspectives 2020*, 2020.
84.   W. Deng, D. Prasad, P. Osmond and F. T. Li, *Journal of Green Building*, 2011, **6**, 96-111.
85.   J. Farfan, M. Fasihi and C. Breyer, *J Clean Prod*, 2019, **217**, 821-835.
86.   K. L. Scrivener, V. M. John and E. M. Gartner, *Cement and Concrete Research*, 2018, **114**, 2-26.
87.   J. Zuo, B. Read, S. Pullen and Q. Shi, *Habitat International*, 2012, **36**, 278-286.
88.   A. Akhtar and A. K. Sarmah, *J Clean Prod*, 2018, **186**, 262-281.
89.   M. R. Munaro, S. F. Tavares and L. Bragança, *J Clean Prod*, 2020, **260**, 121134.
90.   H. A. Abdel-Gawwad, E. Heikal, H. El-Didamony, F. S. Hashim and A. H. Mohammed, *Ceramics International*, 2018, **44**, 7300-7304.

91. *United States Environmental Protection Agency (EPA), Advanced Sustainable Material Management: 2018 factsheet*, 2018.

92. L. Mo and D. K. Panesar, *Cement and Concrete Composites*, 2013, **43**, 69-77.

93. C. Liang, N. Lu, H. Ma, Z. Ma and Z. Duan, *J Co2 Util*, 2020, **39**, 101185.

94. M. Thiery, P. Dangla, P. Belin, G. Habert and N. Roussel, *Cement and Concrete Research*, 2013, **46**, 50-65.

95. D. Zhang, Z. Ghouleh and Y. Shao, *J Co2 Util*, 2017, **21**, 119-131.